Flow Field Computations of Combustor-Turbine Interactions Relevant to a Gas Turbine Engine

Sarah Stitzel[1]

Karen A. Thole

Mechanical Engineering Department,
Virginia Tech,
Blacksburg, VA 24061

The current demands for high-performance gas turbine engines can be reached by raising combustion temperatures to increase power output. High combustion temperatures create a harsh environment that leads to the consideration of the durability of the combustor and turbine sections. This paper presents a computational study of a flow field that is representative of what occurs in a combustor and how that flow field convects through the first downstream stator vane. The results of this study indicate that the development of the secondary flow field in the turbine is highly dependent on the incoming total pressure profile. The endwall heat transfer is also found to depend strongly on the secondary flow field. [DOI: 10.1115/1.1625691]

Introduction

The major contributions to the advances in gas turbine engine performance have been improvements in power output, reliability, and fuel efficiency. The current demands for increasingly higher performance while maintaining affordability and engine durability can be reached through the achievement of hotter combustion temperatures and better cooling schemes. To improve these cooling schemes for both the combustor and the turbine sections, an understanding of the flow field is needed. In particular, an understanding is needed as to how the combustor flow field impacts the heat transfer in the downstream turbine.

Secondary flows that develop in the turbine vane passage lead to detrimental heat transfer on the endwall. These secondary flows are dependent on the incoming radial pressure gradient along the vane span and on the inherent pitchwise pressure gradient between two adjacent airfoils. While past studies have assumed that the spanwise pressure gradient results from a simple turbulent boundary layer along the combustor liner, that assumption is not necessarily correct given the complexity of most combustor designs. The purpose of this research was twofold: to computationally model a nonreacting combustor in order to predict the resulting flow fields, and to determine the effect of these flow fields on the development of the secondary flows in the downstream turbine passage. In particular, one aspect that was investigated was the influence of a backward-facing slot relative to a flush interface between the combustor and turbine section. The uniqueness of this study exists in the fact that combustors and turbines have typically been treated as two independent systems.

Past Studies

For the idealistic case of a flat velocity profile with a simple isothermal turbulent boundary layer along the upstream platform, Langston [1] proposed an accurate representation of the secondary flows that develop in a turbine. A horseshoe vortex is formed by a downward turning of the flow as it approaches the vane leading edge. The pressure side leg of the horseshoe vortex turns into the passage vortex while the suction side leg of the horseshoe vortex is suppressed by the passage vortex as it convects through the passage.

The first studies to have simulated total pressure variations using those variations as the vane inlet conditions were by Schwab et al. [2] and Stabe et al. [3]. These two studies used a combustor exit radial temperature simulator (CERTS), which included circumferential cooling slots with no dilution holes. It was clearly identified from this study that changes occurred in the total pressure profile when using the CERTS as compared to not using the CERTS. Details are not available, however, for comparing any effects that the two different total pressure profiles had on the secondary flow field in the vane section.

Butler et al. [4] showed that the secondary flows within the first vane remained unaffected when the total pressure of the incoming flow was held constant between the cases having and not having a temperature distortion. This is consistent with the theoretical results of Munk and Prim [5], which showed that a constant total pressure leads to no changes in the streamline pattern. Shang and Epstein [6] and Hermanson and Thole [7] both showed computational verification that temperature gradients do not affect the secondary flow patterns in the stator vane section unless the total pressure field is altered.

A few studies have measured endwall heat transfer as a result of injection from a two-dimensional, flush slot just upstream of the vane. Early studies by Blair [8] and Granser and Schulenberg [9] reported measured adiabatic effectiveness levels for a range of blowing ratios. One of the key findings was that the endwall adiabatic effectiveness distributions showed extreme variations across the vane pitch with much of the coolant being swept across the slot toward the suction side corner, resulting in reduced coolant near the pressure side. Measured heat transfer coefficients by Blair [8] were similar between no slot and slot injection cases.

A series of experiments were reported for various injection schemes upstream of a nozzle guide vane with a contoured endwall by Burd and Simon [10], Burd et al. [11], Oke et al. [12], and Oke et al. [13]. In these studies coolant was injected from an interrupted, flush slot that was inclined at 45 deg just upstream of their vane. Similar to others, they found that most of the slot coolant was directed toward the suction side at low slot flow conditions. They also found that a two-dimensional slot was more effective at cooling the downstream vane platform than two rows of discrete film-cooling holes [13].

Kost and Nicklas [14] and Nicklas [15] combined an upstream slot with film-cooling holes in the downstream vane passage to examine the effects of each on the secondary flow field and platform heat transfer at transonic conditions. One of the most interesting results from this study was that they found for the slot flow alone, which was 1.3 percent of the core flow, the horseshoe vortex became more intense. They attributed the strengthening of the

[1]Present address: Techsburg, Inc., 2901 Prosperity Road, Blacksburg, VA 24060.

Contributed by the International Gas Turbine Institute and presented at the International Gas Turbine and Aeroengine Congress and Exhibition, Atlanta, GA, June 16–19, 2003. Manuscript received by the IGTI December 2002; final revision March 2003. Paper No. 2003-GT-38253. Review Chair: H. R. Simmons.

horseshoe vortex to the fact that for the no slot injection the boundary layer was separated with fluid being turned away from the endwall at the injection location.

The only studies involving a slot that was not flush with the endwall surface were the experimental studies reported by Colban et al. [16,17]. They combined the effects of upstream combustor film-cooling holes and slot flow from a backward-facing step. Their results indicated that as the liner film-cooling flow was increased, much of the coolant was transported up the vane surface and resulted in no additional benefit to the downstream turbine endwall.

Computational Methodology

For this study all of the computational fluid dynamics (CFD) simulations were done using a commercial code by Fluent, Inc. (1998). This software package utilizes pressure based flow solvers to model the mass, momentum, and energy conservation equations using either structured or unstructured meshes. All of the solutions were achieved with second-order discretization of the conservation equations. The pressure and velocity were coupled using the semi-implicit method for pressure-linked equations (SIMPLE) algorithm.

Fluent provides the capability of choosing between several turbulence models. Previous studies by Hermanson and Thole [7] of the same geometry used in this research provided a comprehensive turbulence benchmarking study employing the standard k-ε model (Launder and Spalding [18]), the renormalization group (RNG) k-ε model (Yakhot and Orszag [19]), and the Reynolds stress model (RSM) (Launder et al. [20]). Reasonable comparisons between predictions and experiments of the passage secondary flows were achieved using the RNG k-ε model with wall functions. Good agreement was also achieved with the RSM predictions, but the added computational expense was not warranted. Based on these findings and the fact that film cooling and secondary flow development were the primary interest for the study, the RNG k-ε model with nonequilibrium wall functions was used for these computations.

The computational models were all created using primarily tetrahedral mesh elements, with some hexahedral, pyramidal, and wedge elements. The quality of the meshes was determined by the cell skewness. The skewness gives a measure of how far a triangular or quadrilateral (two-dimensional) or tetrahedron (three-dimensional) is from its perfect form, where perfect form is defined as equilateral. A skew of zero is perfect and one is poor. For this model the mesh surface skew was kept below 0.75, with an average value of 0.3. The interior volumetric skew was kept below 0.85 with an average value of 0.4. For all the cases studied grid adaptions were based on three main quantities; velocity gradient, wall unit, and turbulent kinetic energy. Grid independence of a given case was judged based on two main parameters: the total pressure loss at several locations through the combustor and downstream, and adiabatic effectiveness values, η, on the combustor liner. For the combustor model containing a quarter sector (half turbine vane pitch) the change in the total pressure loss was less than 8.5 percent between a grid size of 8×10^5 as compared to 1.1×10^6 cells. The change in the average effectiveness levels just downstream of the dilution holes was less than 1.2 percent between the grids having 8×10^5 and 1.1×10^6 cells. A 9×10^5 cell mesh was considered grid independent for these studies. The final mesh on the vane portion of the domain was created using the grid from Hermanson and Thole [7]. The final mesh sizes, summarized in Table 1, are a combination of the vane grid size plus a full turbine vane pitch.

For all cases computed, the convergence criteria was set such that the residuals decreased by four orders of magnitude for all equations except energy in which the residuals decreased by seven orders of magnitude. Each computation was continued 50–100 iterations beyond convergence to ensure that the residuals continued to decrease steadily and that the solution was actually converged. The vane no-slot case required approximately 950 iterations to reach convergence and took approximately 95 hours (four days) running on four processors. The slot cases required approximately 200–300 more iterations than the no-slot cases to reach convergence. The computations were made on either an SGI Origin 2000 or an SGI Origin 2100 on four parallel processors to increase the speed per iteration.

Table 1 Flow conditions for the three cases studied

Case	1	2	3
Cooling hole geometry	Axial	Axial	Compound
Cells	2.3 million	2.5 million	2.5 million
Domain	1 pitch	1 pitch	1 pitch
		Exit Mass Flow (%)	
Inlet		55	53.6
Dilution 1 top/bottom		8.75/8.75	8.75/8.75
Dilution 2 top/bottom		8.75/8.75	8.75/8.75
Panels 1, 4		1.5/1.5	1.5/1.5
Panels 2, 3		3.5/3.5	3.5/3.5
Exit slot		0/0	0.7/0.7

Boundary Conditions and Test Cases

Three different test cases were modeled in an attempt to understand the effects of the important characteristics of the combustor geometry on the exit flow field and on the endwall secondary flow field. These cases, along with the particular flow conditions, are summarized in Table 1 with the geometrical features indicated in Figs. 1(a) and 1(b). The computational domain for the vane and

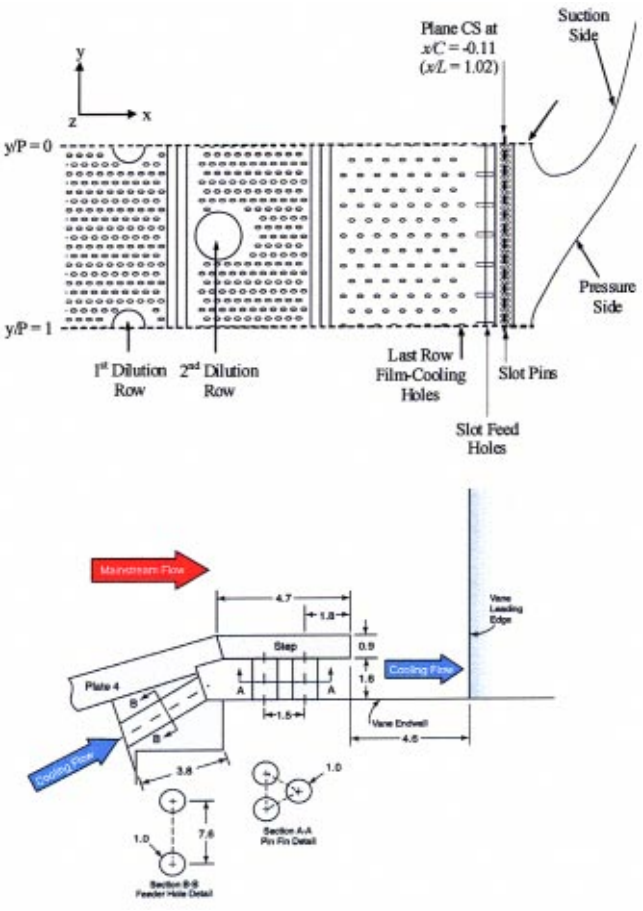

Fig. 1 (Color online) Illustration showing layout for the film-cooling holes and dilution holes relative to the vane location

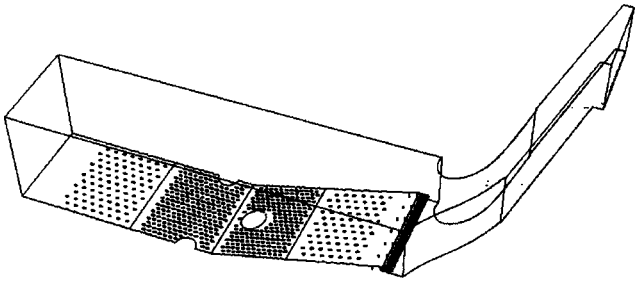

Fig. 2 Schematic of computational domain for a full pitch combustor model for Case 2 with the slot

combustor are shown in Fig. 2. These cases differed from each other only in the geometry of the combustor cooling scheme. The baseline case (Case 1) included film cooling and dilution jets. Case 2 contained film cooling and dilution with an exit slot at the combustor-vane interface. Case 3 included film cooling, dilution, and the exit slot, but with film-cooling holes that were oriented with a 45 deg compound angle in addition to the 30 deg inclination. This compound angle was such that the coolant flow is injected in the same direction as that of the turbine vane. Note that Case 2 had a slightly lower contraction angle (15.5 deg) in the combustor section relative to the baseline case (contraction angle of 17.2 deg). This higher contraction angle was necessary to account for the height of the step. The computational models of the slot cases (Cases 2 and 3) included seven slot feed holes and 52 slot pin fins. The vane stagnation was located 3.6 slot step heights downstream of the trailing edge of the last combustor liner panel.

The inlet boundary conditions to the combustor were set to the proper constant velocity to ensure the correct mass flow rate through the turbine vane giving an exit vane $\mathrm{Re}=1\times10^6$. An outflow boundary condition was used at 1.5 chord lengths downstream of the vane trailing edge. An additional 0.1 chord length was added to the boundary in the streamwise direction to avoid highly skewed cells at the outflow. Symmetry conditions were applied at the midspan while side boundaries were periodic. All surfaces were assumed to have adiabatic boundary conditions. To reduce the mesh size, a velocity boundary condition was applied at the exit of the film-cooling holes. This boundary condition was determined by simulating a single film-cooling hole and plenum with the same momentum flux ratio. The resulting velocity field computed at the inlet of the single hole simulation was applied to all of the film-cooling holes in the liner panels having that same momentum flux ratio (note that the mass flow was conserved through each hole). Each cooling hole contained 144 cells across the surface, giving 1700 cells in the entire hole. A constant mass flow was applied across the inlets for the dilution jets and slot feed holes.

Comparison of Predictions and Measurements

The computations presented in this paper were made for comparison purposes to large-scale experiments using a nonreacting combustor simulator as described by Barringer et al. [21] and Colban et al. [16,17]. Complete measurements of the near wall flows exiting an actual combustor are nearly impossible to achieve in an operating engine. For this purpose, a facility was designed to simulate the geometry and flow conditions of an early design of a prototypical aeroengine combustor with these values being provided by industry (Soechting and Cheung [22]). The purpose of making this facility large scale ($9\times$) was to allow for good spatial measurement resolution. The stator geometry that was placed in a linear cascade has been described in numerous previous studies (Kang and Thole [23]; and Radomsky and Thole [24,25]). The vane was also scaled up by a factor of 9.

As a first step in the computational study, benchmarking of the CFD results against experimental data was done for Case 2, including axial film cooling slots, dilution jets, and exit slot. Comparisons will be made to the measured endwall surface temperatures as described by Colban [16,17]. Endwall surface temperature measurements were taken with an infrared camera and presented as adiabatic effectiveness values.

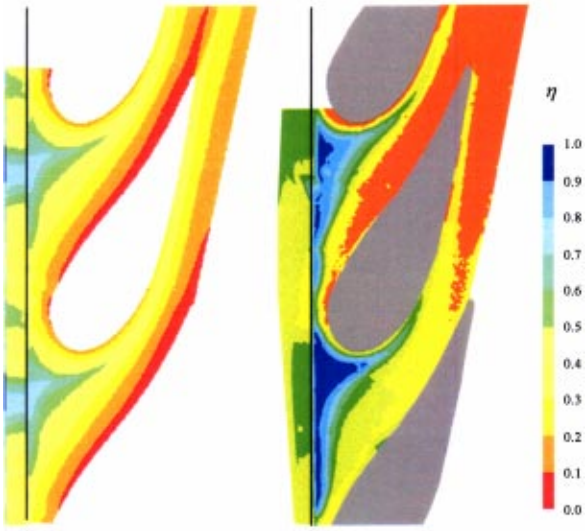

Fig. 3 (Color online) Comparisons of surface adiabatic effectiveness contours for Case 2 with the slot (*a*) predicted using CFD and (*b*) experimentally measured (Colban and Thole [16])

The surface temperature measurements in Fig. 3 show that CFD predicts slightly higher temperatures as compared with the experimental results near the suction surface. The overall results, however, show reasonable agreement, particularly in the critical regions at the leading edge with a warm ring around the vane. The laterally averaged adiabatic effectiveness values through the passage are shown in Fig. 4 where $X/C=0$ is located on the downstream slot edge. The largest differences between the experimental and computational results are seen upstream of the vane where cooler temperatures were measured relative to those predicted. Through the passage the difference between the computational and experimental results is less than 5 percent, which we found to be reasonable agreement.

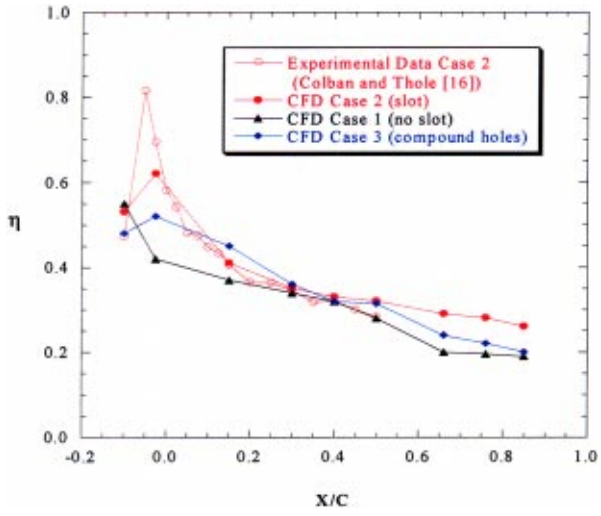

Fig. 4 (Color online) Comparisons of laterally averaged adiabatic effectiveness through the vane passage computationally predicted and experimentally measured

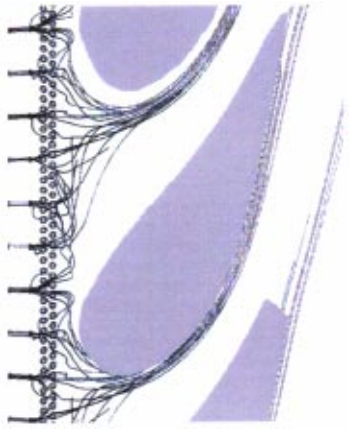

Fig. 5 (Color online) Streamlines released from slot feed holes around vane for Case 2 with a slot

Effects of Exit Slot on Flow Fields

This section will present a discussion of the effects of the slot flow on the combustor exit profile and downstream effectiveness for the no-slot injection (Case 1) and the slot injection (Case 2). Although the coolant available has increased due to the slot for Case 2 relative to Case 1, it is still valuable to compare the effects that the stepped slot has on the overall flow field as well as cooling performance. In addition, comparisons will be made to previous computational results published by Hermanson and Thole [7] for a turbulent boundary layer along the platform approaching the same vane geometry.

Prior to making the secondary flow comparisons, it is important to recognize the dynamics of the slot flow. Figure 5 shows path lines of the flow exiting the slot. Many of these streamlines indicate a flow reversal into the slot. This flow reversal for the slotted

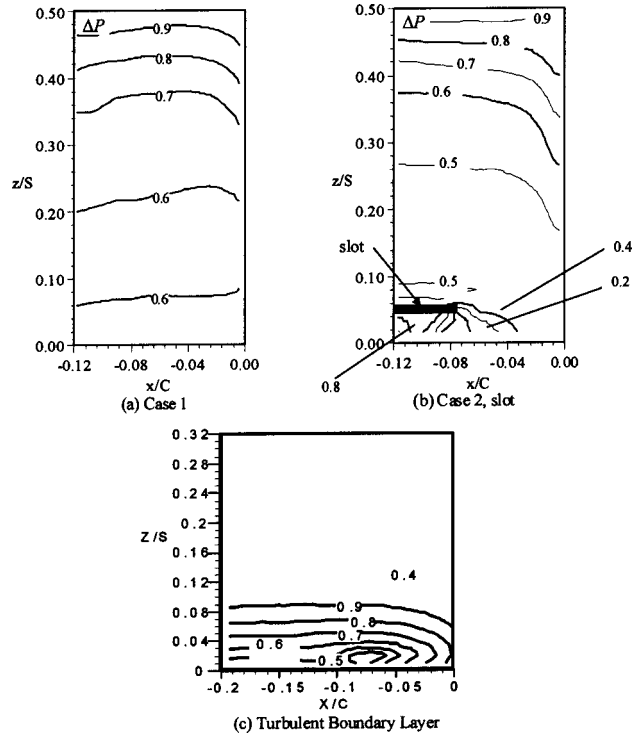

Fig. 6 Total pressure contours in plane SP for (*a*) Case 1, (*b*) Case 2 with the slot and (*c*) an approaching turbulent boundary layer along the endwall [7]

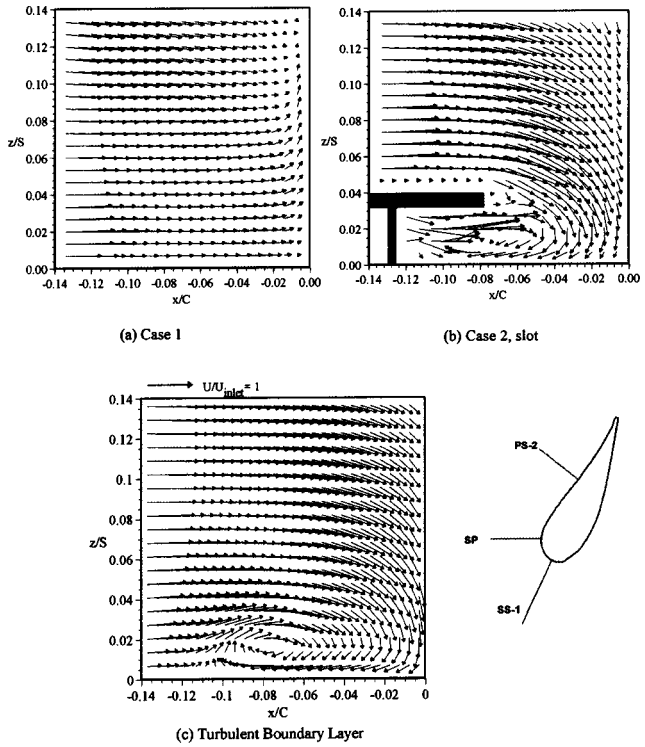

Fig. 7 Velocity vectors in SP for (*a*) Case 1, (*b*) Case 2, and (*c*) turbulent boundary layer [7]

juncture is caused by the fact that there is a much lower total pressure in the slot flow as compared with the flow above the step. The blowing ratio for the slot is quite low at $M=0.24$. Ingestion of the mainstream gas into the slot greatly reduces the effect that the slot could have had on the endwall effectiveness. The endwall streamlines show that all of the flow from the slot was either drawn back under the slot or drawn towards the suction side of the vane.

This flow ingestion can be explained by considering a comparison of total pressure profiles along the vane span in the stagnation plane for the no slot (Case 1) and slot case (Case 2) as compared to an approaching turbulent boundary layer along the platform [7]. These comparisons are shown in Figs. 6(*a*)–6(*c*). The maximum total pressure is located for all of the cases at the vane midspan decreasing towards the endwall. The differences between these cases are in the near endwall region. Case 1 shows an increase in the near-wall region due to the film approaching the vane. This pressure profile and its development as it moves through the vane passage had a distinct effect on the passage secondary flows. Case 2 with the slot shows this same peak due to the film-cooling flow just above the slot, but also shows a significant reduction in the total pressure under the slot. It is this lower total pressure that drives the flow from above the slot into the slot mixing out the slot coolant with a higher temperature gas.

Figures 7(*a*)–7(*c*) show the in-plane flow vectors in a plane that is aligned with the inlet flow direction at the vane stagnation location (plane SP) for the slot and no-slot cases as well as for an approaching turbulent boundary layer. For the turbulent boundary layer case, the leading edge vortex is centered at $x/C=-0.07$ and $z/S=0.015$. For the slot case this vortex was present at approximately the same location. For the no-slot case, however, there was no leading edge vortex that formed. The reason for no leading edge vortex is the fact that the approaching boundary layer has been energized such that there is a relatively flat total pressure profile approaching the vane. These patterns are consistent with what would be expected from the total pressure profiles in the stagnation plane, as shown in Figs. 6(*a*)–6(*c*).

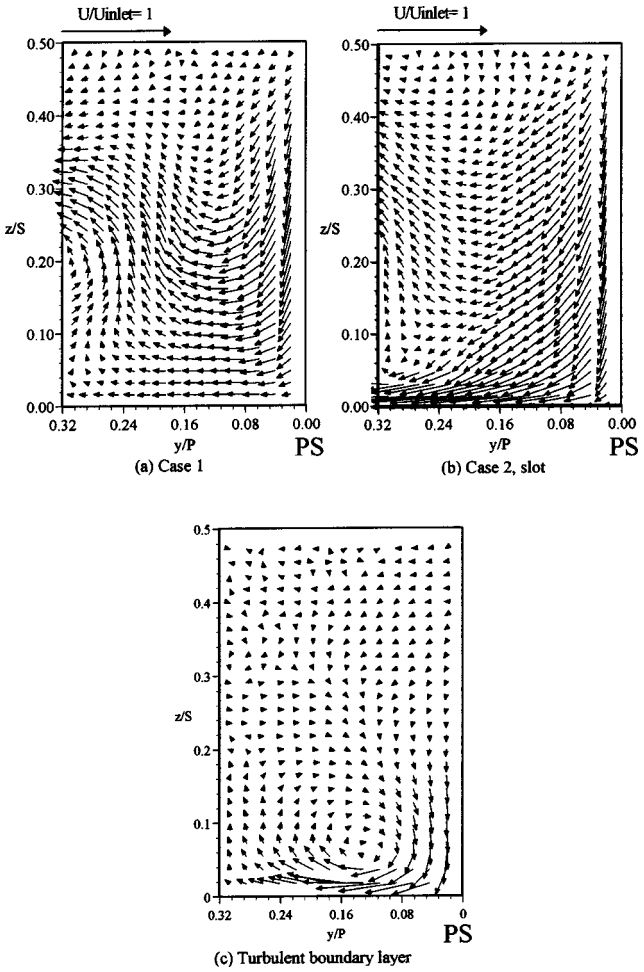

Fig. 8 Secondary flow fields in PS-2 for (*a*) Case 1, (*b*) Case 2, and (*c*) an approaching turbulent boundary layer [7]

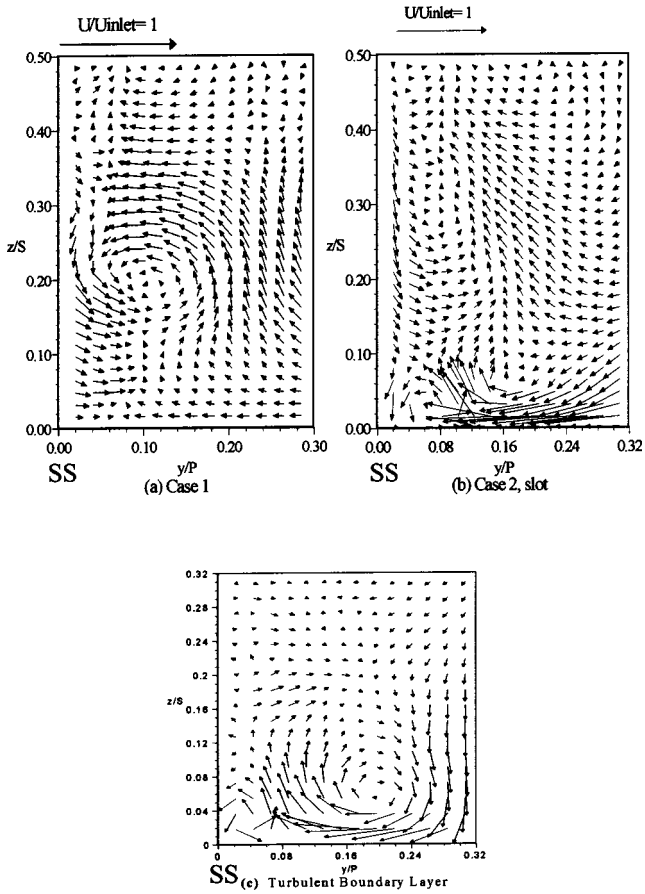

Fig. 9 Secondary flow fields in SS-1 (*a*) Case 1, (*b*) Case 2 with the slot, and (*c*) an approaching turbulent boundary layer along the endwall [7]

Figures 8(*a*)–8(*c*) show a comparison of the secondary flows produced in a plane orthogonal to the pressure side of the vane (PS-2, as illustrated in Fig. 7). The case with the approaching turbulent boundary layer along the endwall produces a clear passage vortex centered at $z/S=0.06$ and $y/P=0.12$. In comparison with the turbulent boundary layer, Case 1 shown in Fig. 8(*a*) indicates a secondary flow pattern that is much different with two vortical patterns near $z/S=0.2$. These vortical patterns can be explained by the change in sign of the total pressure profile at the vane inlet [Fig. 6(*a*)]. There is a minimum in the total pressure near this same span location for Case 1, whereby the secondary flow pattern indicates flow towards this minimum total pressure region. For Case 2 with the slot, however, no complete passage vortex is present in plane PS-2. While similar spanwise motion occurs for both Cases 1 and 2 with downward flows along the suction surface, there is a much stronger velocity across the pitch for Case 2.

Figures 9(*a*)–9(*c*) show a comparison of the secondary flows produced in plane SS-1 for Cases 1 and 2 along with that for a case with the approaching turbulent boundary layer. Again, the secondary flow patterns for these three cases are significantly different. For the case with an approaching turbulent boundary layer, the remnants of the suction side leg of the horseshoe vortex are present as well as the passage vortex from the adjacent vane (this is in good agreement with the model by Langston [1]). For Case 1 with film cooling and no slot, there is a vortex with the same orientation as the suction side leg of the horseshoe vortex, but it is much removed from the endwall being located at $z/S=0.2$. There is no evidence of a vortex having the same orientation as the passage vortex for Case 1. Again this can be explained by the approaching endwall boundary layer being energized. For Case 2, the suction side leg of the horseshoe vortex was clearly visible at $y/P=0.05$, $z/S=0.03$ in plane SS-1 with downward motion along the suction surface. No distinct passage vortex was seen but a weak vortex at $z/S=0.28$ rotating in the opposite direction of a passage vortex was seen similar to Case 1.

The development of the flow through the passage in the near-wall region can be clearly visualized by looking at streamlines released upstream of stagnation at $x/C=-0.05$, as shown in Figs. 10(*a*) and 10(*b*) for Case 1 and Fig. 10(*c*) for Case 2 with the slot. For Case 1 the streamlines showed no secondary vortex development below 13 percent span and showed a slight downward motion along both the pressure and suction surfaces. Figure 10(*b*) shows streamlines released from 15–20 percent of the span for the no slot case at $x/C=-0.05$. The vortical motion centered at approximately 18 percent of the span that was seen in the vector plot in Fig. 9(*a*) can be seen here, whereas no secondary motion was seen in the near-wall streamlines. For Case 2 the path of the suction side horseshoe vortex in Fig. 10(*c*) could be clearly seen, with the streamlines colored by the spanwise velocity component. The flow traveled downward on the pressure side with no clear vortical motion consistent with the secondary flow vector plots. The strong cross-passage flows are clearly seen in the streamlines moving towards the adjacent vane near the endwall.

Effects of Film-Cooling Geometry

Film-cooling hole configurations for the liner of a combustor varies among the different combustor designs. The variation of the

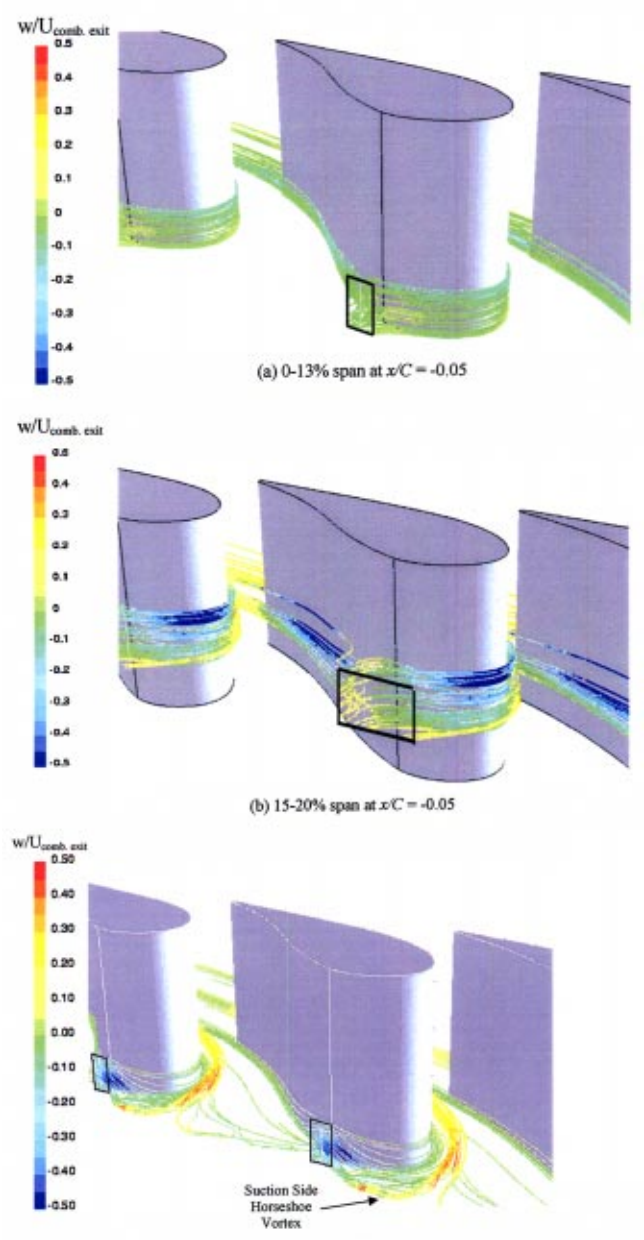

Fig. 10 (Color online) Streamlines released for Case 1 (no slot) colored by $w/U_{comb,exit}$ from (*a*) 0–13 percent span and (*b*) 15–20 percent span. (*c*). Streamlines released at stagnation from 0 to 13 percent of the span at $x/C=-0.05$ for Case 2 with the slot colored by $w/U_{comb,exit}$.

flow field as a result of having a compound angle on the film-cooling hole was predicted computationally for this study (Case 3). The effect of having a compound angle on the resulting, pitchwise-averaged total pressure profile exiting the combustor is shown in Fig. 11 in the stagnation plane. Figure 11 can be compared directly to the axial hole case in Fig. 6(*b*). The general pattern was the same with high pressure at the midspan and a low-pressure region under the slot. For Case 2 with the axial cooling holes, $\Delta P=0.4$ occurred directly above the slot, while for the compound hole case the value on top of the slot increased to $\Delta P=0.6$. The difference in ΔP in this region resulted from the film exiting the cooling holes. This larger total pressure for the compound holes is consistent with the fact that the flow exiting from a hole at a compound angle sees a larger resistance than flow exiting an axial hole and will therefore require a larger total

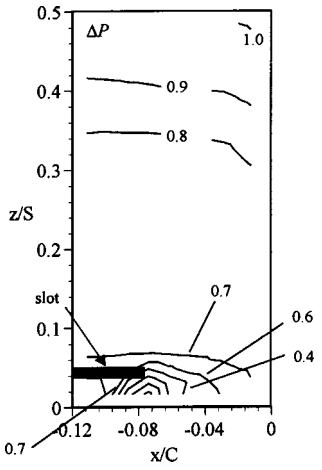

Fig. 11 Total pressure contours in plane SP for Case 3 with a slot and compound angle film-cooling holes

pressure for injection at the same momentum flux ratio. In comparing the compound angle with that of the axial hole for the single hole computations under the same flow conditions, a 22 percent higher total pressure difference between the coolant and mainstream was required for the compound angle hole relative to the axial hole (note that this is relative to the freestream dynamic head). This caused a higher total pressure for the compound hole case above the step. The compound angle film cooling also had an impact on the secondary flow field since it changed the total pressure profile approaching the vane. Figures 12(*a*) and 12(*b*) show the secondary flow field for the compound angle case in planes PS-2 and SS-1, which can be directly compared with Case 2 results shown in Figs. 8(*b*) and 9(*b*). PS-2 flow fields were quite similar with strong motion downward along the vane surface and away from the vane along the endwall. One difference for the compound angled case is an upward motion at $y/P=0.3$ that is not seen for the axial hole case.

More noticeable differences were detected in the secondary flow fields along the suction side of the vane. The secondary flow field indicates that the suction side leg of the horseshoe vortex was clearly visible for both cases with the compound angle case showing a stronger vortex. The compound angle case also showed a distinct passage vortex located at $y/P=0.12$ and $z/S=0.2$ while the axial case did not. The axial case showed additional vortical

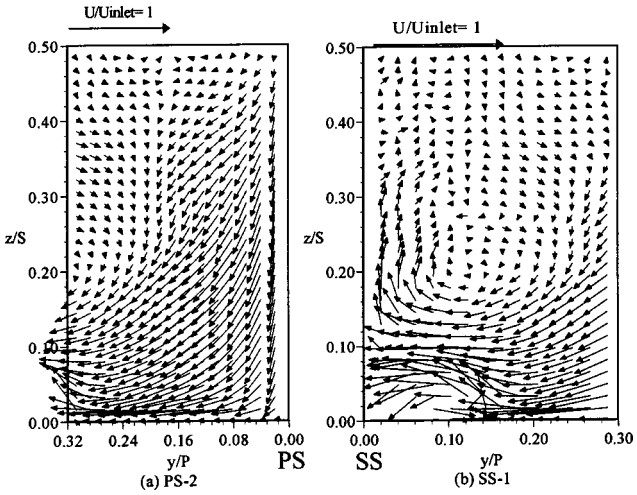

Fig. 12 Secondary flow fields for Case 3 with compound angle film-cooling and slot (*a*) plane PS-2 and (*b*) plane SS-1.

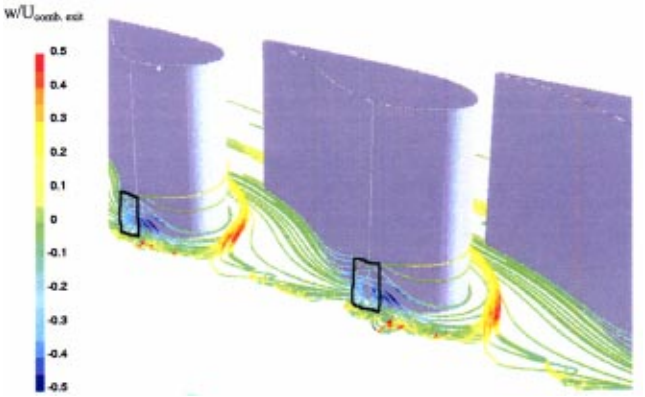

Fig. 13 (Color online) Streamlines released from 0–13 percent span at $x/C=-0.05$ for Case 3 colored by $w/U_{comb,exit}$.

motion in the opposite direction of the passage vortex at $y/P=0.08$ and $z/S=0.28$, which was not present for the compound angle case.

Streamlines released from 0–13 percent of the span at $x/C=-0.05$ are shown in Fig. 13 for Case 3, the compound angle case. The suction side horseshoe vortex is visible as well as the upward motion of the streamlines along the suction surface. The pressure side shows no vortical motion in the near-wall region and downward motion along the surface. These results indicate that in general the effect of the compound angle hole orientation on the secondary flow field was to create stronger vortical motion, particularly on the suction side. This could be attributed to the total pressure profile, which showed a larger pressure gradient in the near-wall region for the compound angle than for the axial cooling hole case.

Comparisons of Adiabatic Effectiveness Levels

The effects of these flow fields on the endwall effectiveness can be seen by looking at the effectiveness contours shown in Figs. 14(*a*)–14(*c*). The laterally averaged adiabatic effectiveness on the endwall for these cases was indicated in Fig. 4. Note that these effectiveness levels use the mass-averaged temperature as the reference temperature for the freestream. Using the mass-averaged temperatures (defined at the exit of the slot), which includes both the dilution and coolant flows, allows direct comparisons to be made between the cases.

For all of the cases, hot spots developed at the leading edge and along the pressure surface towards the trailing edge. For Case 2 with the slot, lower levels of effectiveness occurred at the leading edge and along the pressure side despite the additional coolant as compared with Case 1. Since Case 2 with the slot gave low total pressures near the endwall, the hot mainstream flow was convected downwards onto the endwall. Figure 4 indicates that the laterally averaged values for Case 2 showed increased effectiveness directly after the addition of the slot flow; however through the passage the average effectiveness for Cases 1 and 2 were nearly equal. The decrease in adiabatic effectiveness on the endwall for the compound angle (Case 3) is attributed to the increased secondary flow.

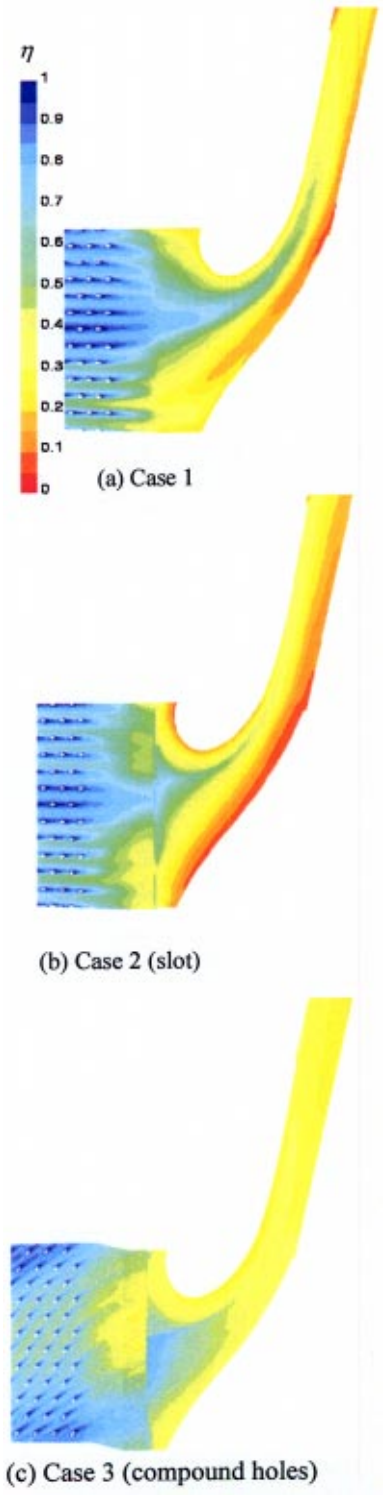

Fig. 14 (Color online) Endwall effectiveness contours for (*a*) Case 1 with no slot, (*b*) Case 2 with slot, and (*c*) Case 3 compound angled film-cooling holes and slot

Conclusions

The combustor-turbine junction has an important effect on the inlet profile for the turbine, particularly in the near-endwall region, which is often difficult to measure. Comparisons were made in this paper for cases with upstream film cooling on the liner panel of the combustor, with the same film cooling and the addition of a slot at the combustor-turbine juncture, and with compound angled film-cooling holes. These cases were compared with the typical assumption of having a two-dimensional, turbulent boundary on the approaching endwall. With the exit slot present the mainstream flow field remained the same as without the exit slot; however, significant changes in the near-wall region occurred. The slot flow produced a significantly low total pressure region from 0 to 5 percent of the span due to the deceleration of the slot flow as it exited the feed holes and pin fin arrangement. In addition, ingestion of mainstream fluid into the slot was predicted.

While the slot introduced additional coolant along the wall, thereby increasing the average adiabatic effectiveness just downstream of the combustor exit, an overall reduction in endwall temperatures further downstream along the endwall were not predicted. This reduction in endwall temperatures was not present due to the secondary flow fields that were predicted to be much stronger for the case with the slot than for the no-slot case.

Changing the orientation of the film-cooling holes from an axial to a compound angle with the turning in the same direction as the vane had a smaller impact on the combustor exit profile than the effect of the slot. The flow exiting the compound angle holes had a higher total pressure than the flow exiting the axial holes. This led to a total pressure profile at the combustor exit for the compound angle case with a higher total pressure over the entire span as compared to the axial case. The compound holes showed a slightly decreased adiabatic effectiveness along the vane endwall due to the stronger secondary flows relative to the axial cooling hole case.

These results all lead to the conclusion that it is a poor assumption to conduct turbine vane flow field studies with a two-dimensional turbulent boundary layer as the incoming condition. A realistic combustor, such as the one studied here, will exhibit a three-dimensional exit flow field with nonuniformities in temperature, pressure, and velocity in both the radial and circumferential directions. Making small changes in the cooling scheme and geometry affect the combustor exit profiles, thereby affecting the vane secondary flow pattern.

Acknowledgment

The authors would like to acknowledge Pratt & Whitney for their support.

Nomenclature

C = true chord of stator vane
D = film cooling hole or slot feed hole diameter
L = combustor length
M = mass flux ratio $= \rho_{jet} V_{jet} / \rho_\infty V_\infty$
Ma = Mach number
p_0 = total pressure
P = pitch
Re = Reynolds number $= C U_{exit} / \nu$
S = span
T, T_{aw} = static and adiabatic temperatures
T_{jet} = coolant temperature
U,V,W = absolute velocity components
u,v,w = local flow plane, transformed velocity components
x,y,z = local coordinate system
X,Y,Z = global, stationary coordinate system
η = adiabatic effectiveness $= (T_{aw} - T_{ave})/(T_{jet} - T_{ave})$
ΔP = normalized total pressure $= 1 - (p_{0,max} - p_0)/(p_{0,max} - p_{s,min})$

Subscripts

ave = mass-averaged value
exit = exit value at midspan
inlet = inlet value at midspan
0 = stagnation value
∞ = freestream value

References

[1] Langston, L. S., 1980, "Crossflows in a Turbine Cascade Passage," J. Eng. Power, **102**, pp. 866–874.
[2] Schwab, J. R., Stabe, R. G., and Whitney, W. J., 1983, "Analytical and Experimental Study of Flow through and Axial Turbine Stage with a Nonuniform Inlet Radial Temperature Profile," AIAA paper no. 83-1175.
[3] Stabe, R. G., Whitney, W. J., and Moffitt, T. P., 1984, "Performance of High-Work Low-Aspect Ratio Turbine Tested with a Realistic Inlet Radial Temperature Profile," AIAA paper no. 84-1161.
[4] Butler, T. L., Sharma, O. P., Joslyn, H. D., and Dring, R. P., 1989, "Redistribution of an Inlet Temperature Distortion in an Axial Flow Turbine Stage," J. Propul. Power, **5**, pp. 64–71.
[5] Munk, M., and Prim, R. C., 1947, "On the Multiplicity of Steady Gas Flows Having the Same Streamline Pattern," Proc. Natl. Acad. Sci. U.S.A., **33**, pp. 137–141.
[6] Shang, T., and Epstein, A. H., 1997, "Analysis of Hot Streak Effects on Turbine Rotor Heat Load," J. Turbomach., **119**, pp. 544–553.
[7] Hermanson, K. S., and Thole, K. A., 2000, "Effect of Inlet Conditions on Endwall Secondary Flows," J. Propul. Power, **16**, pp. 286–296.
[8] Blair, M. F., 1974, "An Experimental Study of Heat Transfer and Film Cooling on Large-Scale Turbine Endwalls," J. Heat Transfer, pp. 524–529.
[9] Granser, D., and Schulenberg, T., 1990, "Prediction and Measurement of Film Cooling Effectiveness for a First-Stage Turbine Vane Shroud," ASME paper no. 90-GT-95.
[10] Burd, S. W., and Simon, T. W., "Effects of Slot Bleed Injection over a Contoured Endwall on Nozzle Guide Vane Cooling Performance: Part I: Flow Field Measurements," ASME paper no. 2000-GT-199.
[11] Burd, S. W., Satterness, C. J., and Simon, T. W., 2000, "Effects of Slot Bleed Injection over a Contoured Endwall on Nozzle Guide Vane Cooling Performance: Part II Thermal Measurements," ASME paper no. 2000-GT-200.
[12] Oke, R., Simon, T., Burd, S. W., and Vahlberg, R., 2000, "Measurements in a Turbine Cascade Over a Contoured Endwall: Discrete Hole Injection of Bleed Flow," ASME paper no. 2000-GT-214.
[13] Oke, R., Simon, T., Shih, T. Zhu, B., Lin, Y. L., and Chyu, M., 2001, "Measurements Over a Film-Cooled, Contoured Endwall with Various Coolant Injection Rates," ASME paper no. 2001-GT-140.
[14] Kost, F., and Nicklas, M., 2001, "Film-Cooled Turbine Endwall in a Transonic Flow Field: Part I—Aerodynamic Measurements," ASME paper no. 2001-GT-0145.
[15] Nicklas, M., 2001, "Film-Cooled Turbine Endwall in a Transonic Flow Field: Part II—Heat Transfer and Film-Cooling Effectiveness Measurements," ASME paper no. 2001-GT-0146.
[16] Colban, W. F., Thole, K. A., and Zess, G., 2002, "Combustor-Turbine Interface Studies: Part 1: Endwall Measurements," ASME paper no. 2002-GT-30526.
[17] Colban, W. F., Lethander, A., T., Thole, K. A., and Zess, G., 2002, "Combustor-Turbine Interface Studies: Part 2: Flow and Thermal Field Measurements," ASME paper no. 2002-GT-30527.
[18] Launder, B. E., and Spalding, D. B., 1974, "The Numerical Computation of Turbulent Flows," Comput. Methods Appl. Mech. Eng., **3**, pp. 269–289.
[19] Yakhot, V., and Orszag, S., 1986, "Renormalization Group Analysis of Turbulence: I. Basic Theory," J. Sci. Comput., **1**, pp. 1–51.
[20] Launder, B. E., Reece, G. J., and Rodi, W., 1975, "Progress in the Development of a Reynolds-Stress Turbulence Closure," J. Fluid Mech., **68**, pp. 537–566.
[21] Barringer, M. D., Richard, O. T., Walter, J. P., Stitzel, S. M., and Thole, K. A., 2002, "Flow Field Simulations of a Gas Turbine Combustor," J. Turbomach., **124**, pp. 508–516.
[22] Soechting, F. O., and Cheung, A., 1999, private communication.
[23] Kang, M., and Thole, K. A., 2000, "Flowfield Measurements in the Endwall Region of a Stator Vane," J. Turbomach., **122**, pp. 458–466.
[24] Radomsky, R. W., and Thole, K. A., 2000, "Flowfield Measurements for a Highly Turbulent Flow in a Stator Vane Passage," J. Turbomach., **122**, pp. 255–262.
[25] Radomsky, R., and Thole, K. A., 2000, "High Freestream Turbulence Effects in the Endwall Leading Edge Region," J. Turbomach., **122**, pp. 699–708.